# Patterns of alteration in chromites from ultramafic rocks of Kudada area, East Singhbhum district (Jharkhand)

Thesis submitted towards the partial fulfilment of the M.Sc. final examination in Applied geology of Jadavpur University, 2019

**Under the guidance of Prof. Sisir K. Mondal**

**By**
**Bijay Kanti Biswas**
**Class roll no. 001720402001**
**Examination roll no. MGEO194002**
**Department of Geological Sciences**
**Jadavpur University, Kolkata- 700032**

*Dedicated to my parents,*
*who were always by my side*

যাদবপুর বিশ্ববিদ্যালয়
কলকাতা-৭০০ ০৩২, ভারত

JADAVPUR UNIVERSITY
KOLKATA-700 032,INDIA

FACULTY OF SCIENCE : DEPARTMENT OF GEOLOGICAL SCIENCES

Certified that **Bijay Kanti Biswas**, Class Roll No. **001720402001**, a student of the M.Sc. Final Year, Department of Geological Sciences, has conducted research work under me for his dissertation thesis on **'Patterns of alteration in chromites from ultramafic rocks of Kudada area, East Singhbhum district (Jharkhand)'**. He has carried out his dissertation under my supervision for the partial fulfillment of the M.Sc. Final Examination (Applied Geology), 2019. This dissertation work is based on hand specimen studies, sample preparation and detailed microscopy (both transmitted and reflected light), EPMA of minerals along with extensive data handling, graphical plots and interpretation of the acquired data. **Bijay Kanti Biswas** has successfully completed his dissertation with sincerity and dedication. The outcome of this research is worth publishing in an International/National Journal as well as presentable to the International conference/ symposium.

Sisir Kanti Mondal
30/5/19

Sisir Kanti Mondal
Supervisor

Dr. Sisir Kanti Mondal
Professor
Department of Geological Sciences
Jadavpur University
Kolkata - 700032

30/05/2019

Head
Department of Geological Sciences
Jadavpur University
Kolkata-700032

দূরভাষ : ২৪১৪-৬৬৬৬/প্রসারণ : ২২৬৮
Website :www.jadavpur.edu
E-mail : hod_geological@jdvu.ac.in
Phone: 2414-6666 Extn. 2268

# Acknowledgement

I would like to thank my supervisor, Professor Sisir K. Mondal, for the immense support and co-operation during my field work, for helping and guiding me throughout the course of my work. I would also like to acknowledge DST-PURSE-PHASE-II, Jadavpur University, and CEFIPRA-Indo-French International Collaborative project 6007-1 to Prof. Sisir K. Mondal for field and analytical support.

# Contents Page

**Abstract**

The ultramafic-mafic rock suite present in Kudada area is located close to the Singhbhum Shear Zone. Although the occurrences of these ultramafic-mafic bodies are reported in some earlier literatures but the detailed research work has not been undertaken so far. The main goal of this study is to find the detail mineralogy of the ultramafic rocks, identify the signatures that modify their primary composition and patterns of alteration in chromite. The major rock types found in Kudada area are talc-magnesite schist with accessory rutile, and serpentinite with accessory chromite. Details studies reveal intense compositional variability in accessory chromites of serpentinite. Core composition of chromites are characterized by high Cr# (≈0.74-0.86) and low Mg# (≈0.15-0.17). Compositional variability on the scale of a single chromite grain occurs in the form of zoning. To identify the pattern of compositional zoning, chromites are subdivided into four types depending on grain size, intensity of fracture and porosity. Smaller (< 20 μm) chromites (type-IV) are highly altered than comparatively larger chromites. Fracture and porosity are mainly developed in larger chromite (type-II) grains. Type-I chromites have medium grain size, less fractured and non-porous verity showing development of two rims. Outermost rim is magnetite surrounds the grey colour ferritchromit rim. Composition of rim-magnetite is similar in all types of chromite but it is compositionally different than the magnetite present in veins. Al, Cr, Mg depleted ferritchromit (R1) is formed surrounding the pore space of type-II chromites. From the texture and mineral chemistry, it is clear that metasomatism by $CO_2$ bearing fluid causes significant increase in the rates of diffusion of the cations and this can facilitate the formation of regular and well-developed ferritchromit rims. Due to later hydrothermal event magnetite rims in all types of chromites and R1 ferritchromit in type-II chromites were formed around the pore spaces.

## 1. Introduction

Chromite is an efficient petrogenetic tool because its chemical composition is controlled by the variation in composition of parental magma which in terns controlled by the mantle melting processes that are typical of particular tectonic settings (e.g., Irvine 1965; Mondal et al. 2006 and references therein). Study of secular changes in chromite composition from different ultramafic-mafic rocks is therefore very useful in understanding the evolution of the Earth's upper mantle through geological time. However, compositional variability is very common in accessory chromites that are present in ultramafic rocks. It may arise due to sub-solidus re-equilibration of the chromites with surrounding silicate minerals and interstitial melt (e.g., Irvine, 1965). Oxidation and alteration of chromite to ferritchromit with magnetite rims is also commonly observed in both layered mafic intrusions and ophiolitic complexes (e.g., Mukherjee et al., 2010; 2015). Similar alteration features are also common in Archean komatiitic volcanic rocks and considered to be related to the serpentinization of the host rock and its subsequent metamorphism (Barnes, 2000; Mondal et al., 2019).

In this dissertation work I have conducted detailed petrographic and mineralogical study of ultramafic-mafic rocks which are present at or near the Kudada village (22°42'43.97"N, 86°11'56.71"E) located at the south of Tatanagar town in the state of Jharkhand (eastern India). Exposures of various sized ultramafic-mafic bodies comprising of chlorite-talc-tremolite-carbonate schist and serpentinite are present in different parts of the Singhbhum Shear Zone (SSZ, **Fig. 1**). One of such ultramafic-mafic rock body is traceable from the west of Surda to Jaduguda area and another ultramafic-mafic body occurs at Kudada area, south of Tatanagar town (**Fig. 2**). Smaller ultramafic-mafic bodies are also present in Mosaboni-Pathargarah areas and several other places in the SSZ, west of Tatanagar. The ultramafic-

mafic rock suite which is present in the Kudada area is located within 7-8 km from the Singhbhum Shear Zone (**Fig. 2**). Although the occurrences of these ultramafic-mafic bodies are reported in some earlier literatures the detailed research work has not been undertaken so far (e.g., Sarkar, 1984). There are no detailed petrographic, mineralogical, petrological and geochemical information available on these ultramafic-mafic rock suite. The absolute and relative ages and the genesis of this ultramafic-mafic rock suite are also not known so far. It is also a debatable issue that this ultramafic rock suite is part of the Early to Mesoarchean Iron Ore Group (IOG) or the Late Archean Dhanjori Group.

In this particular study, detailed investigation of ultramafic body has been carried out by systematic sampling from outcrops, petrographic study using optical microscope (both under reflected and transmitted light) and mineral analyses by Electron Probe Micro-Analyzer. The main goal of this study is to find the detail mineralogy of the ultramafic rocks, identify the signatures that modify their primary composition, patterns of chromite alteration and the role of shearing and concomitant felsic intrusions (e.g., Arkasoni granite) in alteration and genesis of this rock.

## 2. Regional Geology

The Indian shield has four cratons, three of these (Dharwar, Baster, Singhbhum) present in southern block and Bundelkhand craton present in the northern block (Radhakrishna Naqvi, 1986). The Singhbhum Craton (40,000 $km^2$) is situated in eastern India between the latitudes of 21°00'N and 23°15'N and the longitudes of 84°40'E and 86°45'E (**Fig. 1**). The Singhbhum Craton is bounded in the north by the Chhotanagpur Craton, forming the eastern extension of the Satpura mobile belt. The craton is separated from the Satpura mobile belt by Tamar-Porapahar shear zone **(Fig. 1)**. To the south, the craton is bounded by

the Eastern Ghat mobile belt with a tectonic contact marked by the Sukinda Shear Zone (**Fig. 1**). To the east, the Singhbhum Craton is covered under alluvium of the Bengal Basin. Paleoarchean to Mesoarchean granite/gneiss basement rocks known as the Singhbhum Granite Batholithic Complex (SGBC) is the main lithounit in the Singhbhum Craton (Saha, 1994). Older Metamophic Group (OMG) is considered the oldest supracrustal sequence in the Singhbhum Craton. The oldest age of the OMG is constrained by $^{207}Pb/^{206}Pb$ ion microprobe age of ≈3.5 Ga, obtained from detrital zircon belonging to the quartzite unit at Champua area, Orissa (Mishra et al, 1999). The Older Metamorphic Tonalitic Gneiss (OMTG) consists of medium-grained tonalitic to granodioritic gneisses (Saha, 1994). The U-Pb analyses of xenocrystic zircons from the OMTG at Champua area by SHRIMP reveal ages in the range of 4.24-4.03 Ga (Chaudhuri et al., 2018). The OMG consists of both igneous and sedimentary rocks which are metamorphosed to low-grade amphibolite facies. The field relations indicate that the OMG and the OMTG were deformed and metamorphosed before the intrusions of the SGBC granitic rocks (Saha, 1994). The voluminous granitic rocks of the SGBC were emplaced in two phases; the older emplacement age is ≈3.45-3.44 Ga (SBG-A) and the latter phase of emplacement is constrained at ≈3.35-3.32 Ga (SBG-B) (Upadhyay et al., 2014). Other major supracrustal unit in the Singhbhum Craton is known as the Iron Ore Group (IOG) that comprises the three Archean greenstone belts: (i) the Gorumahishani-Badampahar belt, (ii) the Noamundi–Jamda–Koira belt and (iii) the Tomka–Daitari belt (Mondal, 2009). The IOG supracrustal rocks are composed of low- to medium grade metasediments including phyllites, tuffaceous shale, banded iron formation (BIF, ≈120 m thick), ferruginous quartzite, dolomite, and ultramafic-mafic volcanics as well as ultramafic-mafic sill-like intrusives (Saha, 1994; Mondal et al., 2001, 2007; Ghosh and Mukhopadhyay, 2007; Mukhopadhyay et al., 2008). Mukhopadhyay et al. (2008) obtained a SHRIMP U-Pb

age of 3506.8 ± 2.3 Ma from zircons in the dacitic lava within the IOG supracrustal sequence belonging to the Tomka-Daitari greenstone belt. Basu et al. (2008) obtained a 3.4- Ga zircon U-Pb age from the volcanic rocks belonging to the western IOG in the Noamundi-Jamda-Koira greenstone belt.

The Dhanjori Basin formed unconformably over the Archaean basement and is the oldest sedimentary basin in the Singhbhum Craton (Saha, 1994). Dhanjori Group is a terrestrial, primarily fluvial sequence composed of clastic sedimentary rocks overlain by mafic–ultramafic volcanic and volcaniclastic rocks (Mazumder, 2005; Bhattacharya and Mahapatra, 2007). Mishra and Johnson (2005) reported 2858 ± 17 Ma Pb–Pb age for the volcanic rocks of the Dhanjori formation. Chaibasa formation, the lower sequence of the Singhbhum Group is stratigraphically above the Dhanjori Group (Mazumder, 2005). The Dhanjori Group is comprised of tidal sandstones, heterolithic facies and an offshore shale facies (Eriksson et al., 2006). The Dhalbhum formation is unconformably overlying the Chaibasa formation. It is composed of a layer of phyllites, shales, and quartzites overlain by volcanic tuff (Eriksson et al., 2006). The Dalma Group of rocks conformably overlies the Dhalbhum formation and consists of ultramafic-mafic volcanic rocks (e.g., Mazumder, 2005).

Singhbhum Shear Zone (SSZ) is a fold-thrust belt (**Fig. 2**) along which shearing took place around 1600 Ma (e.g., Sengupta and Chattopadhya, 2004; Mazumder et al., 2012). The shear zone rocks underwent two different phase of metamorphism (e.g., Sarkar, 1984; Bandyopadhyay, 2003; Sengupta et al., 2005). Prograde metamorphism (M1) culminated in epidote-amphibolite facies led to the formation of garnet and chloritoid porphyroblast in the pelitic schists. The peak metamorphic P-T estimated from the pelitic rocks in SSZ is 480±40°C and 6.4±0.4 kbar (Bandyopadhyay, 2003; Sengupta et al., 2005). Sengupta et al. (2005) interpreted that retrograde metamorphism (M2) to hydrous mineral assemblage

took place near the peak metamorphic temperature, a process that might reflect a control by fluid influx rather than cooling.

There are number of younger granitic plutons intruding the Singhbhum Mobile belt (SMB), e.g, Kuilapal granite on the East, Mayurbhanj granite, Soda granite, Arakasoni granite, Chakradharpur granite and Tamper kola granite on the west (Sastry et al. 2011). The Arkasoni granite gneiss occurs as detached elongated outcrop close to the northern margin of the Chakradharpur granite gneiss. Age of the Arkasoni granite is about 1052 Ma (Sengupta et al., 1994).

## 3. Geology of the ultramafic-mafic rock from Kudada area

Exposures of talc-carbonate schist and Serpentinite found in Talsa and Ukam pahar respectively at Kudada, south of Tatanagar. These ultramafic mafic rock hills of Kudada area is located within 8-10 Km form Singhbhum Shear Zone. The length and width of the ultramafic-mafic bodies is around 11Km and 3 Km respectively. These ultramafic mafic volcanic rocks are associated with meta sedimentary rock (quartzite). Kudada ultramafic rock body trending almost east-west and becoming gabbroid westward. The relationship between the gabbroid and ultramafic rocks is not obvious. In the ultramafic body veins and veinlets of magnetite and asbestos are common. Patches of talc-carbonate schists are exposed in the open pits at the base of the Talsa pahar, west of Kudada, associated with metabasite rocks. In lumps, the rock is light green coloured, schistose fine grained with soapy feel and readily reacted with HCl. Ultramafic rock(s), now serpentinised, is seen on the north-west slope of Ukam pahar, associated with hematite-quartzite rocks and lies at the northern outskirt of Singhbhum granite (Mukhopadhyay, 1968).

## 4. Methodology

### 4.1. Sampling

Systematic sampling from different location has been conducted to trace the rock type variation of Kudada ultramafic mafic unit. Total 10 sample were collected among which four samples of talc carbonate schist from exposed open pit at the base of Talsa Pahar, five samples of serpentinite from north west exposure of Ukam pahar, one sample from intercalated quartzite unit within serpentinite. Then all samples collected from the field were studied in hand specimen.

### 4.2. Slide preparation

At first samples were cut into 3 slices and cleaned very well by soap water. Among these three slices one was kept for sample preparation, one for future use and one for preparing slide. The slice used for slide preparation was cut again in the shape of a slide and sent to laboratory for thin section preparation. Then this thin polished sections were extensively studied in both transmitted and reflected light microscope. Chromite grains from serpentinite and rutile grains from talc schist were analysed by electron microprobe using a CAMECA SX-100 instrument at the Department of Geology and Geophysics, Indian Institute of technology Kharagpur, operated at 15-kV acceleration voltage with 20-nA probe current, using beam size of 1µm. The standards used were: Na-Albite, Mg-Periclase, Si-Orthoclase, Ca-CaO, Ti-Rutile, Cr-$Cr_2O_3$, Ba-$BaSO_4$, Al-Corundum, Mn-Rhodonite, Fe-Hematite, V-Pure vanadium, Zn-ZnS. The compositions of chromites were recalculated to cationic proportions using calculation scheme of Droop (1987).

## 5. **Petrography**

### 5.1. Hand specimen description

***Talc magnesite schist*** - Talc carbonate schist rocks belonging to Talsa pahar area of Kudada are represented by the samples SHB-18-01, SHB-18-02, SHB-18-03, SHB-18-04. They consist of talc (85-90%), carbonate (5-7%), quartz (1-5%), black colour not identified grains (~1%). Talc is identified by pale green colour, hardness less than 2.5 and one set perfect cleavage. Talc shows flaky nature and forms the schistosity of the rock. Carbonates and quartz are present as veins within the talc schist rocks. Carbonates are readily reacted with HCl. Black colour tiny grains are non-magnetic in nature and showing metallic lustre. There is very low abundance of these grains in sample SHB-18-02, SHB-18-03, and SHB-18-04 with respect to sample SHB-18-01 (**Figs. 3a, b**).

***Serpentinite*** - Serpentinite rocks belonging to Ukam pahar area of Kudada are represented by SHB-18-05, SHB-18-06 SHB-18-07, SHB-18-09, SHB-18-10. The rocks consist of serpentinite (85-92%), chlorite (3-5%), spinel (3-4%) and carbonates (1-2%). The rocks are massive and showing overall deep brownish green colour. Different verities of serpentine present within this rock (**Fig. 3c, d, f**). Dark colour massive verity of serpentine having hardness greater than 3.5 occupy 60-70% of the rock. Chromites are dark brown colour and very weakly magnetic in nature. Very small grains of chromites are disseminated within the serpentinite. Numerous veins of varying thickness (from few mm in sample SHB-18-05 to few cm in sample SHB-18-06, SHB-18-10) are occurred within the rocks which are filled by fibrous verity of serpentinite (chrysotile), chlorite and magnetite. Carbonates are generally occurred as veins and reacted with HCl.

**Microscopic study**

***Talc-magnesite schist*** - The rocks consist of talc (90-95 vol%), magnesite (3-5 vol%), quartz (1-2 vol%), rutile and zircon (< 1 vol%). The rock is highly deformed, and schistose (**Fig. 4a**). The schistosity are formed by talc. Talc forms flaky crystal which is colourless to pale green matrix in plane polarized light. It shows variegated interference colour in crossed polars. Magnesite generally occur as veins within the groundmass of talc which are fine grained and shows anomalous 4$^{th}$ order interference colour under crossed polars. Very small amount of quartz is present as vein and also as disseminated grains with indistinct grain boundary with in the host of talc and magnesite. (**Fig. 4b**)

Small discrete grains of rutiles and zircons are present as accessory phases and scattered throughout the rock (**Fig. 4c**). Rutiles are fine gained, rounded to subrounded in shape, showing dark coffee brown colour in plane polarized light. The abundance of rutiles and zircons are highest in the sample SHB-18-01 with respect to other samples. The rutiles are clustered together to form larger grains (≈ 350 μm) in samples SHB-18-02 and SHB-18-03. Greenish coloured chlorite are developed around the grains of clustered rutile. Zircons are very small (2-3 μm) but clearly visible in BSE image. These are generally associated with the rutile grains.

***Serpentinites*** - The rocks consist of serpentine (90-92%), chlorite (3-5%), magnesite (1-2%) and oxides (1-3%). The rocks are highly deformed, showing crude schistosity and veined by magnesite. Antigorite is the major constituent in serpentinite (80-85%) with veins of chrysotile (10-20%) cut across antigorite. Carbonates also presents as vein within the rock (**Fig. 4e**). Small discrete grains of magnetite are either disseminated or concentrated in serpentine veins. Thick vein (0.5 cm) of chrysotile, chlorite and magnetite present in SHB-18-10 sample (**Fig. 4f**).

Chromite occurs as an accessory mineral in the serpentinite. Chromite grains are subhedral to subrounded in shape, have corroded margins and surrounded by chrome chlorite (**Fig. 4d**). Larger (>150 μm) chromite grains are highly fractured and porous than the smaller ones. In reflected light and in scanning electron microscopic (SEM) study, chromite grains exhibit strong compositional zoning. Depending on grain size, variation in compositional zoning, fracture intensity and porosity, chromites are classified into four type:

**Type-I chromites -** Medium grain size (<150 μm), Less fractured and less porous variety of chromites show the development of two outer rim. Here, the outer rim of highest reflectance surrounds the inner rim which is lighter grey in colour, having lower reflectance. The central part is identified as remnant, less altered chromite. The inner rim is ferritchromit, whereas the outer rim is identified as magnetite. The boundary between core and ferritchromit rim is not very prominent but the contact between ferritchromit rim (r1) and magnetite rim (r2) is sharped. The outer rim has highly irregular contact with surrounding chrome-chlorite. Very few magnetite grains occur as a disseminated manner around the zoned chromite (**Fig. 5a, b**).

**Type-II chromites -** Larger (>150 μm), Highly fractured and porous variety of chromite shows three rim instead of two (**Fig. 5c, d**). Pore spaces mainly filled with chrome chlorite. Around the dark grey and non-porous core of chromite, there is a very light grey colour and porous rim (R1) of ferritchromit followed by comparatively dark grey colour (less dark than core) and non-porous rim (R2) of ferritchromit. The outermost rim (R3) is magnetite shows brighter reflectance. The boundaries between core, R1, R2, and R3 are sharp and prominent. Modal abundance disseminated magnetite around the highly fractured chromite is much larger than previous variety.

**Type-III chromites:** Small, moderately fractured and less porous grains of chromites which are clustered together to form microscopic bands of chromite within serpentinized matrix (**Fig. 5e**). These grains show only one rim around the dark grey core. **Type-IV chromites:** Fine (<20 μm) verity of chromites which are disseminated within the serpentinized matrix (Dashed white circle in **Fig. 5b, c, d, e**). These chromite grains are highly altered in nature.

## 6. Mineral Chemistry

***Compositional profile of zoned chromite***- Zoned chromite grains have studied to determine the elemental distribution (both major and minor elements) across the grain. **Type-I chromites:** Major oxides $Cr_2O_3$, $Al_2O_3$, MgO show progressive loss towards rim which is accomplished by strong enrichment of $Fe_2O_3$. FeO shows negligible change from core to outermost rim (**Fig. 6a**). In minor oxides, ZnO and MnO exhibit similar trend and show strong enrichment in ferritchromit rim (ZnO≈1.05 wt.% and MnO≈2.17 wt.%) and sharply loss towards core (ZnO≈0.02 wt.% and MnO≈0.27 wt.%), and magnetite rim (ZnO≈0.0 wt.% and MnO≈ 0.08 wt.%). $TiO_2$ and $V_2O_3$ exhibit similar trend and show gradual enrichment form core ($TiO_2$≈1.77 wt.% and $V_2O_3$≈0.33 wt.%) to ferritchromit rim ($TiO_2$≈2.13 wt.% and $V_2O_3$≈0.44 wt.%). Sharp loss of $TiO_2$ ($TiO_2$≈0.16 wt.%) and $V_2O_3$ ($V_2O_3$≈0.15wt.%) in magnetite rim is also reported **(Fig. 6a).** In **type-II chromites** $Cr_2O_3$, $Al_2O_3$ and MgO are enriched in R2 but depleted in porous rim R1. The outermost magnetite rim shows similar composition like magnetite rim of type-I chromites **(Fig. 6b).** Minor oxides like ZnO, MnO, $TiO_2$ and $V_2O_3$ are enriched in R2 but depleted in R1. Outermost rim shows similar composition like outermost magnetite rim of type-I chromites **(Fig. 6b). Type-III chromites:** Major oxides composition in type-II chromite cores have $Cr_2O_3$ (≈19.2-20.1 wt.%), $Fe_2O_3$ (≈30.0-32.7 wt.%), $Al_2O_3$ (≈11.2 wt.%) and MgO (≈0.7-1.0 wt.%). Outer magnetite rim has

compositionally similar to outermost rim of type-I and type-II chromites **(Fig. 6c). Type-IV chromites:** These are Cr bearing magnetite contents $Cr_2O_3$ (≈1.4-1.6 wt.%), $Al_2O_3$ (≈0.01 wt.%) and MgO (≈0.1-0.5 wt.%), lower $Fe_2O_3$ (≈63 wt.%). These Cr-bearing magnetite have similar composition with outermost magnetite rims of previous chromites.

Secondary magnetite present along chrysotile-chlorite veins show different chemical composition relative to magnetite present around the outermost rim of accessory chromites. Vein magnetite is depleted in $Al_2O_3$, MgO, MnO, $TiO_2$, $Cr_2O_3$, $V_2O_3$, NiO, ZnO and enriched in $Fe_2O_3$ with respect to rim magnetite.

***Mineral chemistry of all chromites*** - Accessory chromites present in serpentinite are characterized by high *Cr*-number (0.36-1.00) and low *Mg*-number (0.17). The core of the chromites are also extensively altered and showing very high value of *Cr*-number. In Cr-Al-$Fe^{3+}$ triangular plot accessory chromite shows $Al^{3+}$ enrichment trend from core to ferritchromit rim **(Fig. 7d, e).** The plots of *Mg*-number vs. $Fe^{3+}/(Cr+Al+Fe^{3+})$ for all chromites shows (**Fig. 7a**) strong enrichment of $Fe^{3+}$ in the ferritchromit and magnetite rims and fall within the fields of metamorphogenic magnetite and ferritchromit rim as proposed by Barnes and Roeder (2001). The *Cr*-number of primary igneous magnetite is distinct from that of magnetite modified by metamorphism (Barnes, 2000). According to Barnes (2000) the *Cr*-number is low for primary igneous magnetite, because at the stage when magnetite appears on the liquidus of mafic magmas there is little Cr (Cr < 100ppm) but still a significant amount of Al present in the melt. Thus primary igneous magnetite plots at lower right of *Cr*-number vs *Mg*-number and along the Al-$Fe^{3+}$ join of Cr-Al-$Fe^{3+}$ triangular plot. So, magnetite present in the studied samples are not the primary igneous magnetite rather it was formed during metamorphism or later hydrothermal alteration. Chromite tend to lose Al, relative to Cr, during metamorphism and reaction with silicates and metamorphic fluids to form chlorite or

amphibole. This results the R1 rim of type-II spinel to plot along the Cr-$Fe^{3+}$ join of Cr-Al-$Fe^{3+}$ **(Fig. 10b)** and at the top right corner of *Cr*-number vs *Mg*-number plot **(Fig. 7a).**

Altered chromite grains show two distinct trend in Mg ratio vs MnO content. (1) the less altered part (core) of zoned chromite shows a distinct negative trend, that means with Mg ratio increase there is a successive decrease in MnO content. (2) the rim or altered part of the same grain shows enrichment of both MnO with Mg-ratios and a distinct positive trend. **(Fig. 8a)**. *Mg*-number vs ZnO also showing similar trend like *Mg*-number vs MnO. **(Fig. 8b).** $TiO_2$ and $V_2O_3$ against *Mg*-number plot show similar pattern and exhibit bimodal clustering of data **(Fig. 8c).** In $TiO_2$ vs *Mg*-number one cluster is formed in high *Mg*-number (Mg# ≈ 0.12-1.7) having $TiO_2$ content (≈0.5-1.9 wt.%) and another cluster is formed in low *Mg*-number (Mg# ≈ 0.05) having $TiO_2$ content (≈0.0- 2.1 wt.%). $V_2O_3$ vs *Mg*-number plot indicate bimodal clustering of data. One cluster is formed when *Mg*-number is high (≈0.12-0.16) having $V_2O_3$ content about (≈0.11-0.15 wt.%). Another cluster is formed when *Mg*-number is low (≈0.0-0.05) having $V_2O_3$ content about (≈0.1-0.5 wt.%) **(Fig. 8d).**

***Mineral chemistry of zoned chromites*** - Core of **type-II chromites** show more pristine character (enriched in $Cr_2O_3$ and $Al_2O_3$ but depleted in $Fe_2O_3$) than the **type-I chromites (Fig. 10a, b)**. In triangular plot Cr-Al-$Fe^{3+}$ clearly shows that the core of the **type-II chromites** are enriched in Al than **type-I chromites**. Ferritchromit rim 1 of **type-I chromites** are compositionally similar with ferritchromit rim 2 of **type-II chromite**. R1 rim is depleted Al and fall in the Cr-$Fe^{3+}$ joining line of Cr-Al-$Fe^{3+}$ ternary plot **(Fig. 10a, b).** In $Fe^{3+}$-ratio vs MnO plot show gradual enrichment of MnO from core to ferritchromit rim (R1 of **type-II chromites** is depleted in MnO) and sharp decrease of MnO in outermost magnetite rim for all types of chromites **(Fig. 10c, d)**. $Fe^{3+}$# vs ZnO plot shows similar pattern like $Fe^{3+}$-ratio vs MnO plot **(Fig. 10e, f)**. In $Fe^{3+}$# vs $TiO_2$ plot exhibit a negative trend from core to rim. $TiO_2$

values are high in core of **type-I chromite** but there is a wide range of values of $TiO_2$ (≈0.6 to 1.3 wt.%) in case of **type-II chromites (Fig. 10g, h)**. MnO vs *Mg*-number plot, having distinct negative trend from core to ferritchromit rim and positive trend from ferritchromit rim to magnetite rim **(Fig. 10i, j)**. ZnO have similar trend like MnO with *Mg*-number **(Fig. 10k, l)**.

## 7. Discussion

Diffusion rate of the trivalent cations are relatively slow with respect to bivalent cations that helps to develop compositional gradient in chromite grain (Rollinson, 1995), which we see as zoning. Fluid activity causes incorporation of Mn and Zn from the surrounding olivine grains during serpentinization, while Al and minor Cr are lost from chromite forms chrome–chlorite around the grain boundary and the pore spaces of altered chromite (Barnes, 2000). Fluids also contribute in bringing about Ti-enrichment in the ferritchromit rims, during serpentinization. The rounded nature of the core indicates that the alteration to ferritchromit had occurred uniformly from all directions (Bliss, 1975). The distinct trend of Al-loss followed by loss of Cr and strong enrichment of $Fe^{3+}$, that is characteristic of ferritchromit (Evans and Frost, 1975) is clearly observed in the Cr–Al–$Fe^{3+}$ diagram **(Fig. 10a).** During ferritchromit formation, the $Fe^{3+}$ content of the chromite grains increases due to prevalence of oxidation conditions. (e.g., Mitra et al., 1992). Formation of ferritchromit has been thought to be linked to either serpentinization process (e.g., Burkhard, 1993) or metamorphism in greenschist to lower amphibolite grade (Barnes et al., 1998). Burkhard, (1993) studied the chromites in the serpentinites from the eastern Central Alps and interpreted the alteration of the spinel to be a function of serpentinization and not metamorphism. Metamorphism was thought to cause only re-crystallization of the spinel.

According to Bliss and MacLean (1975), the ferritchromit formation within Precambrian serpentinite was due to a combination of initial serpentinization that caused the development of magnetite rims around chromite, followed by later metamorphism of the assemblage, and reaction of the magnetite rims with the chromite cores to produce the Al- and Mg-poor ferritchromit rim. Loferski (1986) considered the formation of crystallographically controlled intergrowths of ferritchromit plus chlorite, in the accessory chromites of the Red Lodge District, Montana, to be a product of late stage alteration during serpentinization. Extensive formation of ferritchromit occurring along with crystallographically controlled chlorite in the chromite grains, within a breccia zone of the Mesoarchean Nuasahi ultramafic–mafic complex, eastern India is considered to be a product of metasomatism (Mondal and Zhou, 2010). Interaction of the chromitite fragments with fluid-rich evolved boninitic magma is considered to have formed the ferritchromit within the Nuasahi breccia zone. Ferritchromit is also common in the serpentinized dunite of the lower ultramafic unit in Nuasahi, which formed during hydrothermal alteration of the ultramafic-mafic complex due to interaction with evolved seawater (Mondal et al., 2003).

In this current study, the irregular and patchy occurrences of ferritchromit indicate that no crystallographic orientation has been followed for their formation and that the alteration is heterogeneous. These irregular and patchy occurrences probably formed by oxidation in a late hydrothermal episode. This is because the alteration is observed to occur mainly along grain boundaries or fractures through which grain-fluid interaction can easily occur. The alteration occurs to be strongest in **type-I, III and IV** chromites because these chromites are modally insignificant, and are surrounded by hydrous magnesian silicates (serpentine) with which they can easily exchange cations (Burkhard, 1993). Metamorphism also plays an important role and cause regular zoning in the **type-I chromite** grains. These grains show

both the regular occurrence of well-developed ferritchromit rims around grain boundary **(Fig. 5a, b).** Metamorphism causes significant increase in the rates of diffusion of the cations, and this can facilitate the formation of regular and well-developed ferritchromit rims. Metamorphism also enables equilibration of the chromite core with the surrounding silicate assemblages, due to enhanced diffusion (Barnes, 2000). In all the types of chromite grains the $TiO_2$ content shows negative correlation with $Fe^{3+}$# **(Fig. 10g, h).** The positive correlation of MnO with $Fe^{3+}$# from core to ferritchromit rim of all the chromite grains (**type-I, II and III**) may be attributed to the incorporation of Mn from carbonates which are common within the altered ultramafic rocks. Later stage hydrothermal fluid content less amount MnO, for this reason MnO vs $Fe^{3+}$# show a negative correlation from ferritchromit rim to magnetite rim. ZnO vs $Fe^{3+}$# plot exhibit a very strong enrichment in only ferritchromit rim (r1 for **type-I** and R2 for **type-II**). Core values of $TiO_2$ of **type-II chromites** are compositionally similar with the stranded unaltered chromites values. So enrichment of $TiO_2$ in ferritchromit rim is definitely linked with incorporation of $TiO_2$ in later hydrothermal activity.

Compositional modification of the chromite grains depends also on the size of the grain and fracturing (scale of deformation) they suffer. The smallest grains of **type-IV** and **type-III** chromites are compositionally more modified compared to the relatively larger (<150 µm) **type-I chromite** grains. The same is observed for the highly deformed and fractured grains of **type-II chromites**. This irregular and heterogeneous nature of compositional variation clearly indicates that $Fe^{3+}$ rich ferritchromit rim (R1) of **type-II chromites** and outermost Cr-bearing magnetite is definitely related to low temperature hydrothermal alteration of the ultramafic-mafic complex.

## 8. Conclusion

From the texture and mineral chemistry of all types of accessory chromites in serpentinized matrix, it is clear that the rock suffered metasomatism which altered the original composition of ultramafic rocks and formed antigorite-rich serpentinite. Metasomatism had introduced a high diffusion rate of element-exchange between accessory chromites and silicate matrix. Due to metasomatism related to shearing event of the Singhbhum Shear Zone (SSZ), the ferritchromit rims were formed. During formation of ferritchromit rim Cr, Al, Mg were lost from the chromite that were compensated by the gain of Zn, Mn and $Fe^{3+}$. Cr, Al, Mg were incorporated in to the chlorite that formed during metasomatism. Then due to hydrothermal alteration the outermost rims were formed in **type-I chromites**. Due to comparatively larger size the **type-II chromites** carried the signatures of deformation before hydrothermal alteration. Due to deformation the porosity was formed (**Fig. 5c, d**). Then through the pore spaces the hydrothermal solution was percolated and formed R1 ferritchromit rim in **type-II chromite**. Later within the pore space, chlorite formed and consumed higher amount of Al and little amount of Cr and Mg **(Fig. 11a). Type-IV chromites** were formed by the fragmentation of larger chromite grains (**Fig. 11b**). Low temperature fibrous verity of serpentine (chrysotile) and chlorite filled up the open fractures and formed perpendicularly against the boundary of the fractures.

## References


Acharyya, S.K., 1993. Greenstones from Singhbhum Craton, their Archaean character, oceanic crustal affinity and tectonics. Proc. Natl. Acad. Sci. India 63 (A), 211–222

Barnes SJ (2000) Chromite in Komatiites. II. Modification during greenschist to mid-amphibolite facies metamorphism. J Petrol. 41:387–409

Barnes SJ (2006) Komatiites: petrology, volcanology, metamorphism, and geochemistry. Econ Geol Special Publication 13, pp 13–49

Barnes SJ, Roeder PL (2001) The range of spinel compositions in terrestrial mafic and ultramafic rocks. J Petrol 42:2279–2302

Barnes, Stephen. (1998). Chromite in Komatiites 1. Magmatic Controls on Crystallization and Composition. Journal of Petrology. 39

Basu, A.R., Bandyopadhyay, P.K., Chakrabarti, R., Zou, H., 2008. Late 3.4 Ga Algoma-type BIF in the Eastern Indian Craton. Geochimica et Cosmochimica Acta. 72

Bliss NW, MacLean WH (1975) The paragenesis of zoned chromite from central Manitoba. Geochim Cosmochim Acta 39:973–990

Burkhard DJM (1993) Accessory chromian spinels: their coexistence and alteration in serpentinites. Geochim Cosmochim Acta 57:1297–1306

Chaudhuri, Trisrota & Wan, Yusheng & Mazumder, Rajat & Ma, Mingzhu & Liu, Dunyi. (2018). Evidence of Enriched, Hadean Mantle Reservoir from 4.2-4.0 Ga zircon xenocrysts from Paleoarchean TTGs of the Singhbhum Craton, Eastern India. Scientific Reports. 8

Devaraju TC, Alapieti TT, Kaukonen RJ, Sudhakara TL (2007) Chemistry of Cr-spinels from ultramafic complexes of western Dharwar craton and its petrogenetic implications. J Geol Soc India 69:1161–1175

Evans BW, Frost BR (1975) Chrome-spinel in progressive metamorphism—a preliminary analysis. Geochim Cosmochim Acta 39:959–972

Irvine TN (1965) Chromian spinel as a petrogenetic indicator. Part I, Theory. Can J Earth Sci 2:648–671

Irvine TN (1967) Chromian spinel as a petrogenetic indicator. Part II, Petrographic applications. Can J Earth Sci 4:71–103

Loferski PJ (1986) Petrology of metamorphosed chromite bearing rocks from the Red Lodge District, Montana. US Geol Surv Bull 1626-B:B1–B34

Mishra, S, Domuarari, M.P,Wiedenbeck, M.,Goswami, J.N.,Ray, S.,Saha, A.K., 1999. 207Pb/ 206Pb zircon ages and the evolution of the Singhbhum Craton, eastern India: an ion microprobe study. Precambrian Research 93, 139–151

Mitra S, Pal T, Maity PK, Moon HS (1992) Ferritchromit and its optochemical behavior. Mineral J 16:173–186

Mondal SK, Ripley EM, Li C, Frei R (2006) The genesis of Archean chromitites from the Nuasahi and Sukinda massifs in the Singhbhum craton, India. Precambrian Res 148:45–66

Mondal, Sisir & Baidya, Tapan & N Gururaja Rao, Kolar & Glascock, Michael. (2001). PGE and Ag mineralization in a breccia zone of the Precambrian Nuasahi ultramafic-mafic complex, Orissa, India. The Canadian Mineralogist. 39. 979-996

Mondal, Sisir & Frei, Robert & Ripley, Edward. (2007). Os isotope systematics of mesoarchean chromitite-PGE deposits in the Singhbhum Craton (India): Implications for the evolution of lithospheric mantle. Chemical Geology - CHEM GEOL. 244. 391-408

Mondal, Sisir & Khatun, Sarifa & M. Prichard, Hazel & Satyanarayanan, Manavalan & Ravindra Kumar, G R. (2018). Platinum-group element geochemistry of boninite-derived Mesoarchean chromitites and ultramafic-mafic cumulate rocks from the Sukinda Massif (Orissa, India). Ore Geology Reviews. 104

Mondal, Sisir. (2009). Chromite and PGE deposits of Mesoarchean ultramafic-mafic suites within the greenstone belts of the Singhbhum Craton (India): implication for mantle heterogeneity and tectonic setting. Journal of the Geological Society of India. 73. 36-51

Mukherjee, R., Mondal, S.K., Rosing, M.T., Frei, R., 2010. Compositional variations in the Mesoarchean chromites of the Nuggihalli schist belt, Western Dharwar Craton (India): potential parental melts and implication for tectonic setting. Contrib. Mineral. Petrol. 160, 865–885

Mukherjee, Ria & Mondal, Sisir & González-Jiménez, Jose & Griffin, W & J. Pearson, Norman & O' Reilly, SY. (2015). Trace-element fingerprints of chromite, magnetite and sulfides from the 3.1 Ga ultramafic–mafic rocks of the Nuggihalli greenstone belt, Western Dharwar craton (India). Contributions to Mineralogy and Petrology. 169:59

Mukhopadhyay, Joydip & Beukes, Nicolas & Armstrong, Richard & Zimmermann, Udo & Ghosh, Gautam & A. Medda, R. (2008). Dating the Oldest Greenstone in India: A 3.51-Ga Precise U-Pb SHRIMP Zircon Age for Dacitic Lava of the Southern Iron Ore Group, Singhbhum Craton. Journal of Geology - J GEOL. 116. 449-461

Mukhopadhyay, Joydip & Ghosh, Gautam & Beukes, Nicolas & Gutzmer, J. (2007). Precambrian colluvial iron Ores in the Singhbhum craton: Implications for origin, age

of BIF-hosted high-grade Iron Ores and stratigraphy of the Iron Ore group. Journal of the Geological Society of India. 70. 34-42

Pal, Dipak & Barton, Mark & Sarangi, Dr. Akshaya. (2009). Deciphering a multistage history affecting U–Cu(–Fe) mineralization in the Singhbhum Shear Zone, eastern India, using pyrite textures and compositions in the Turamdih U–Cu(–Fe) deposit. Mineralium Deposita. 44. 61-80

Radhakrishna, B.P., Naqvi, S.M., 1986. Precambrian continental crust of India and its evolution. Journal of Geology 94, 145–166

Rollinson H (1995a) Composition and tectonic settings of chromite deposits through time. Econ Geol 90:2091–2092

Rollinson H (1995a) Composition and tectonic settings of chromite deposits through time. Econ Geol 90:2091–2092

Saha, A.K., 1994. Crustal evolution of Singhbhum North Orissa, East-ern India. Geol. Soc. India Memoir 27, 341

Sarkar S (1984) Geology and ore mineralisation of the Singhbhum copper-uranium belt, Eastern India

Sengupta N, Mukhopadhyay D, Sengupta P, Hoffbauer R (2005) Tourmaline-bearing rocks in the Singhbhum shear zone, eastern India: evidence of boron infiltration during regional metamorphism. Am Mineral 90:1241–1255

Sengupta S, Ghosh SK (1997) The kinematic history of the Singhbhum shear zone. Proc Indian Acad Sci A Earth Planet Sci 106:185–196

Upadhyay, Dewashish & Chattopadhyay, Sabyasachi & Kooijman, Ellen & Mezger, Klaus & Berndt, Jasper. (2014). Magmatic and Metamorphic History of Paleoarchean Tonalite—Trondhjemite—Granodiorite (TTG) Suite from the Singhbhum Craton, Eastern India. Precambrian Research. 252. 180-190

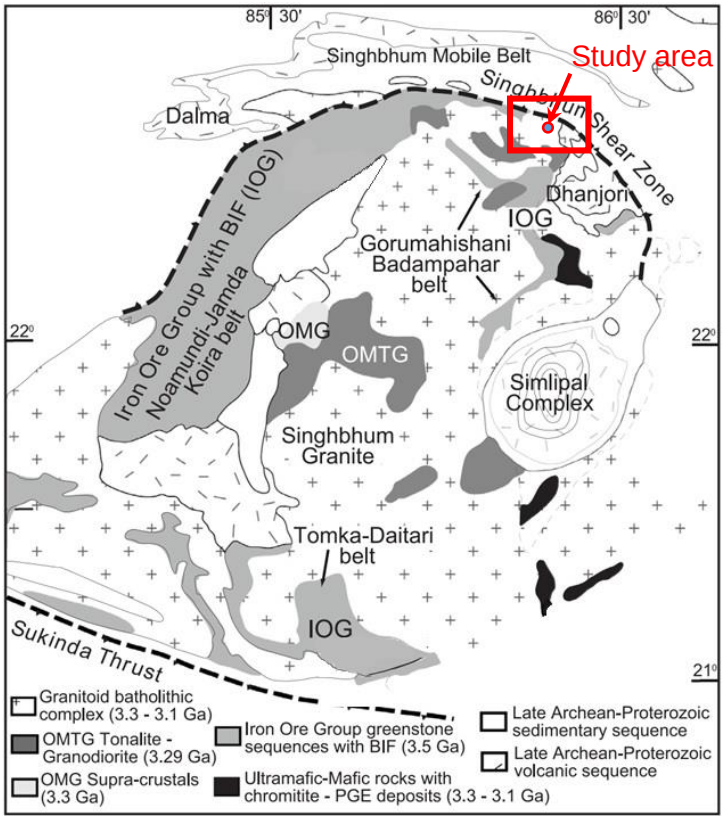


**Fig. 1** Geological map of the Singhbhum Craton, India (Saha, 1994; Sengupta et al., 1997; Mondal et al., 2019)

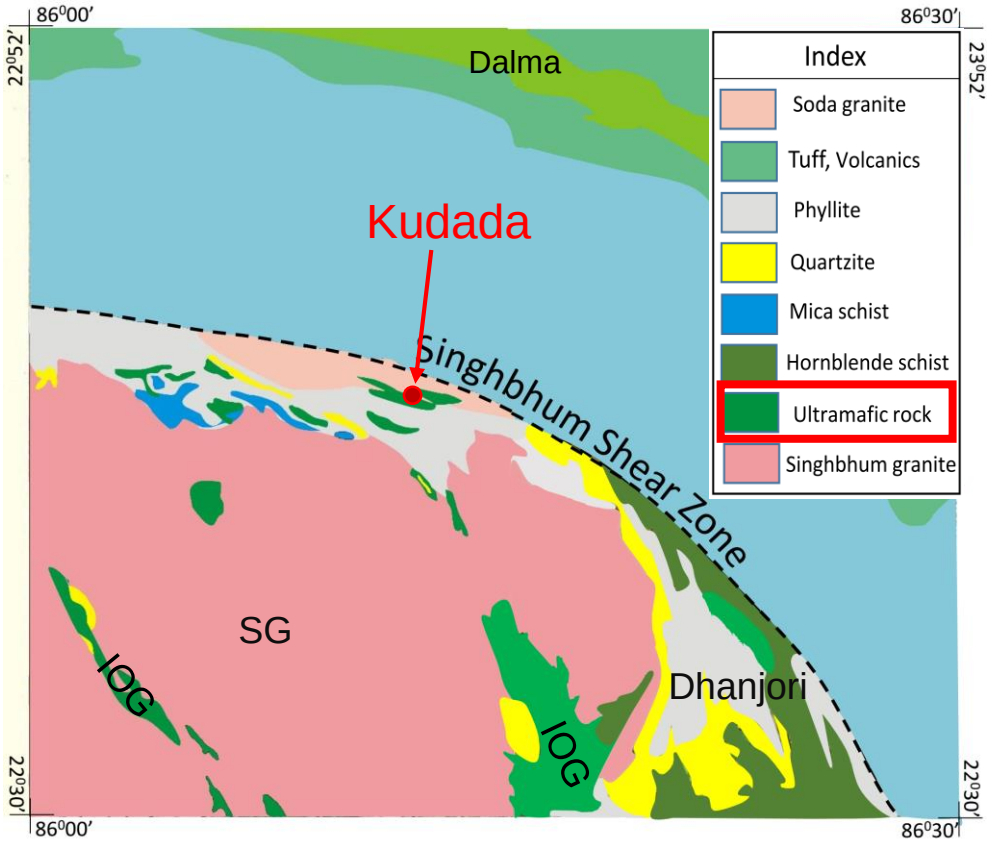


**Fig. 2** Lithological map of eastern part of Singhbhum- Shear Zone (SSZ) (after geological map of Singhbhum Craton, Jamshedpur quadrangle GSI, 1998)

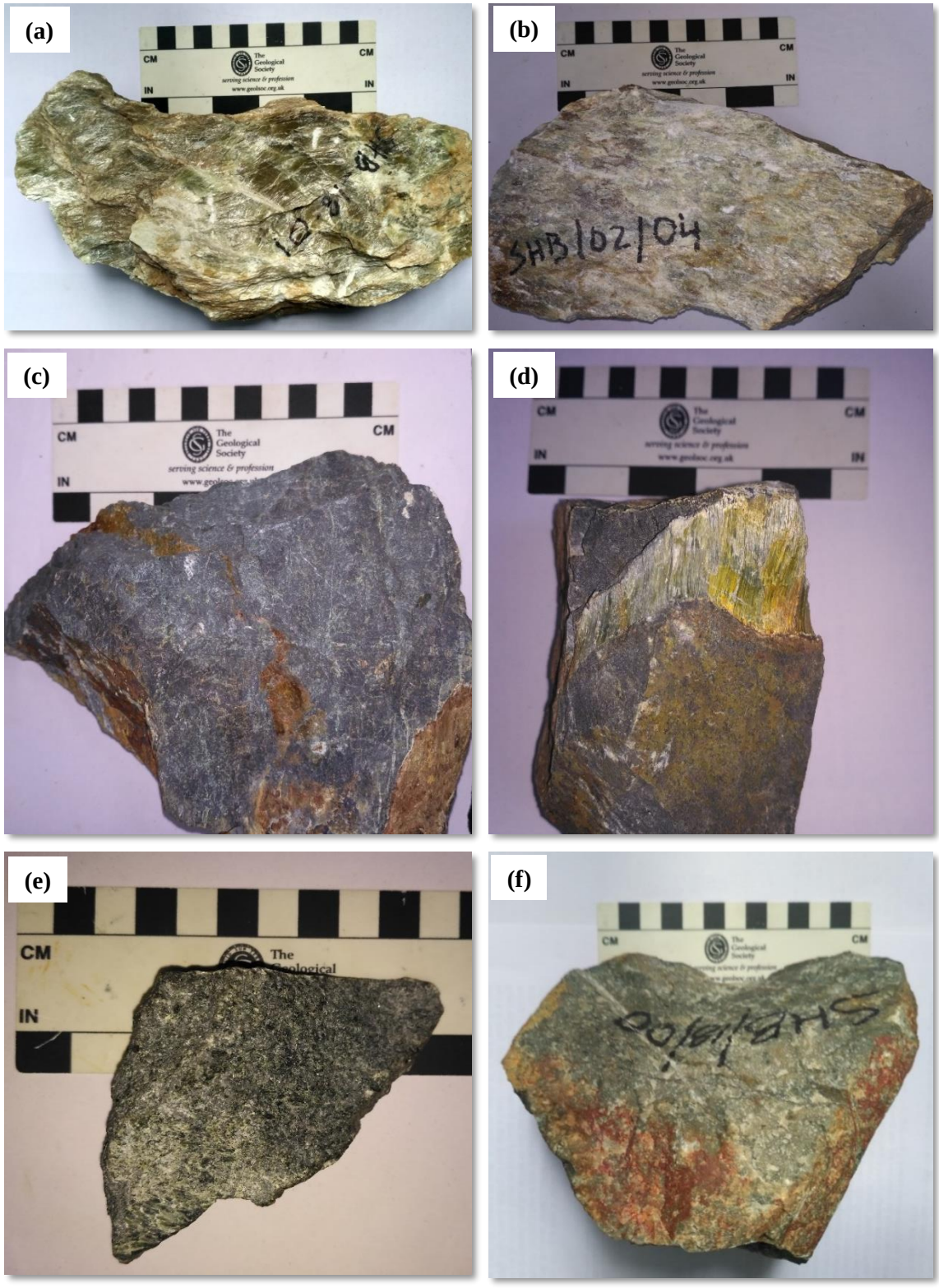


**Fig.3** Photograph of hand specimens illustrating different rocks type. **(a, b)** Talc-carbonate schist having numerous quartz vein with it**. (c, d, e)** Serpentinite having veins of chrysotile, chlorite and magnetite. **(f)** Quartzite.

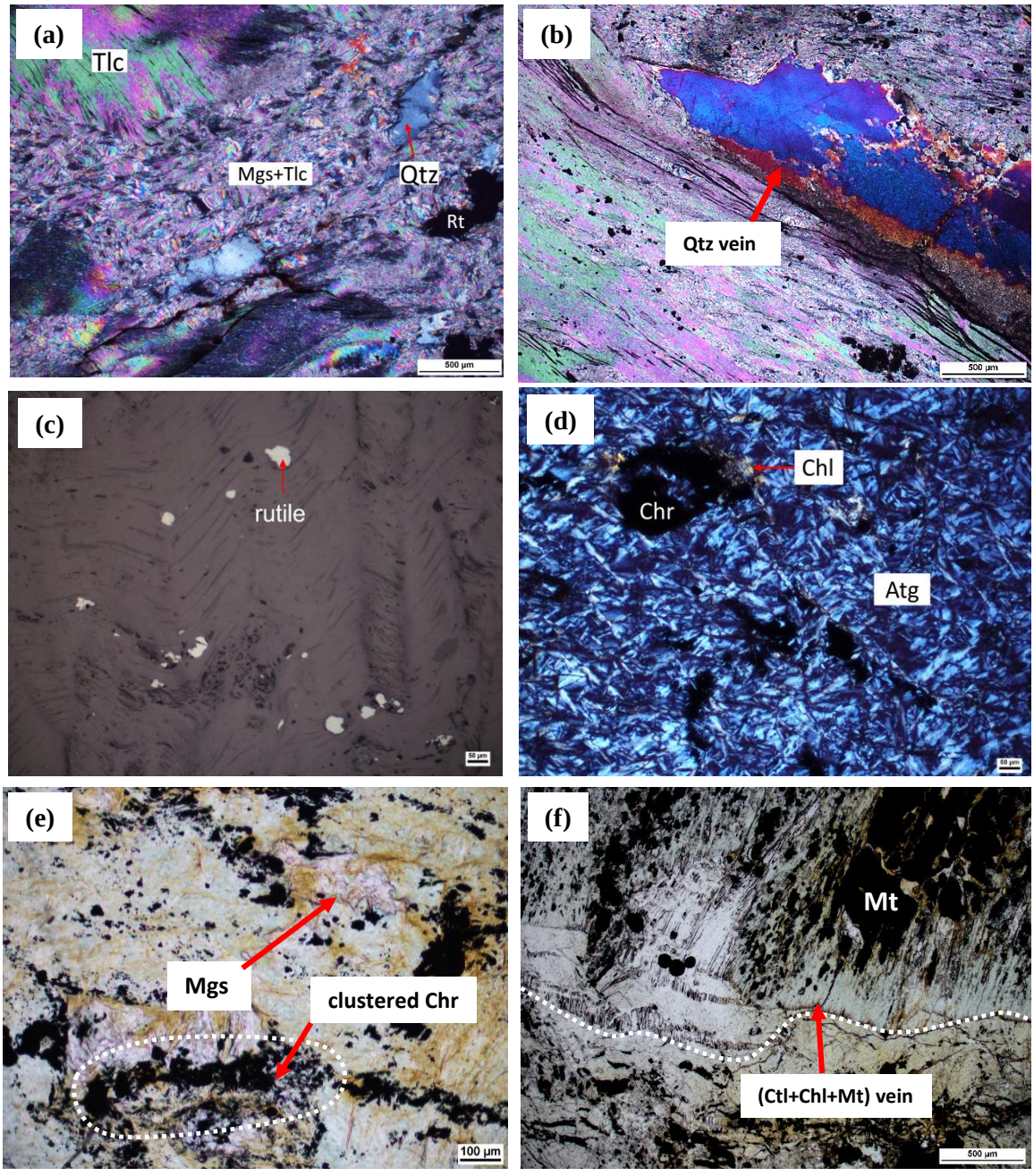


**Fig. 4** (**a)** Photomicrograph of talc-carbonate schist. Disseminated quartz is formed within magnesite and talc matrix. **(b)** Quartz vein within talc-carbonate matrix. **(c)** Accessory rutile in talc-magnesite schist **(d)** Chromite within antigorite host. Cr-Chl is formed around the chromite. (**e)** Microscopic band of clustered chromite within antigorite-magnesite schist. **(f)** Thick vein (0.5 cm) of ctl+chl+mt within host rock (sample SHB-18-10).

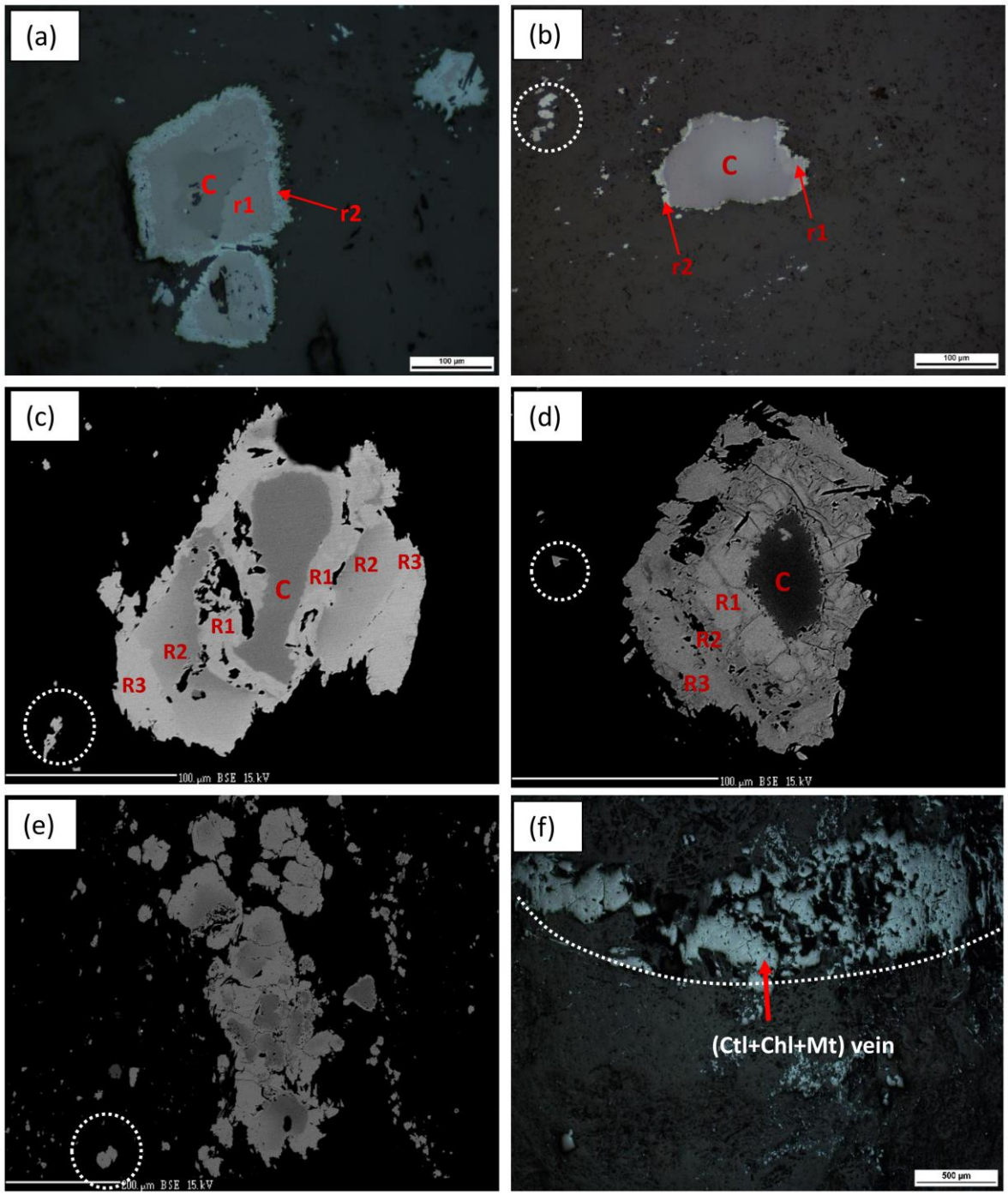


**Fig. 5 (a, b) Type-I chromites:** Photomicrograph of Less fractured variety of chromite show the development of two outer rim around the core. The outer rim of *Mt* (r1) surrounds the inner rim of *Fcmt* (r2). (a- Sample SHB-18-06, b- Sample SHB-18-05). **(c, d) Type-II chromites:** BSE image of Highly fractured variety of chromite shows three rim. Around the dark grey core of chromite, there is a very light grey rim of *Fcmt* (R1) followed by comparatively dark grey *Fcmt* (R2) to *Mt* (R3). (c- Sample SHB-18-05, d- Sample SHB-18-06). **(e) Type-III chromites:** BSE image of band of chromite with *Fcht* core and *Mt* rim (sample SHB-18-06). **(f)** BSE image of secondary magnetite in the chrysotile chlorite vein (right side of the image) and disseminated smaller *Fcht* and *Mt* within serpentine. (sample SHB-18-10) . [Dotted white circle in b,c,d,e represents **Type-IV chromites.**]

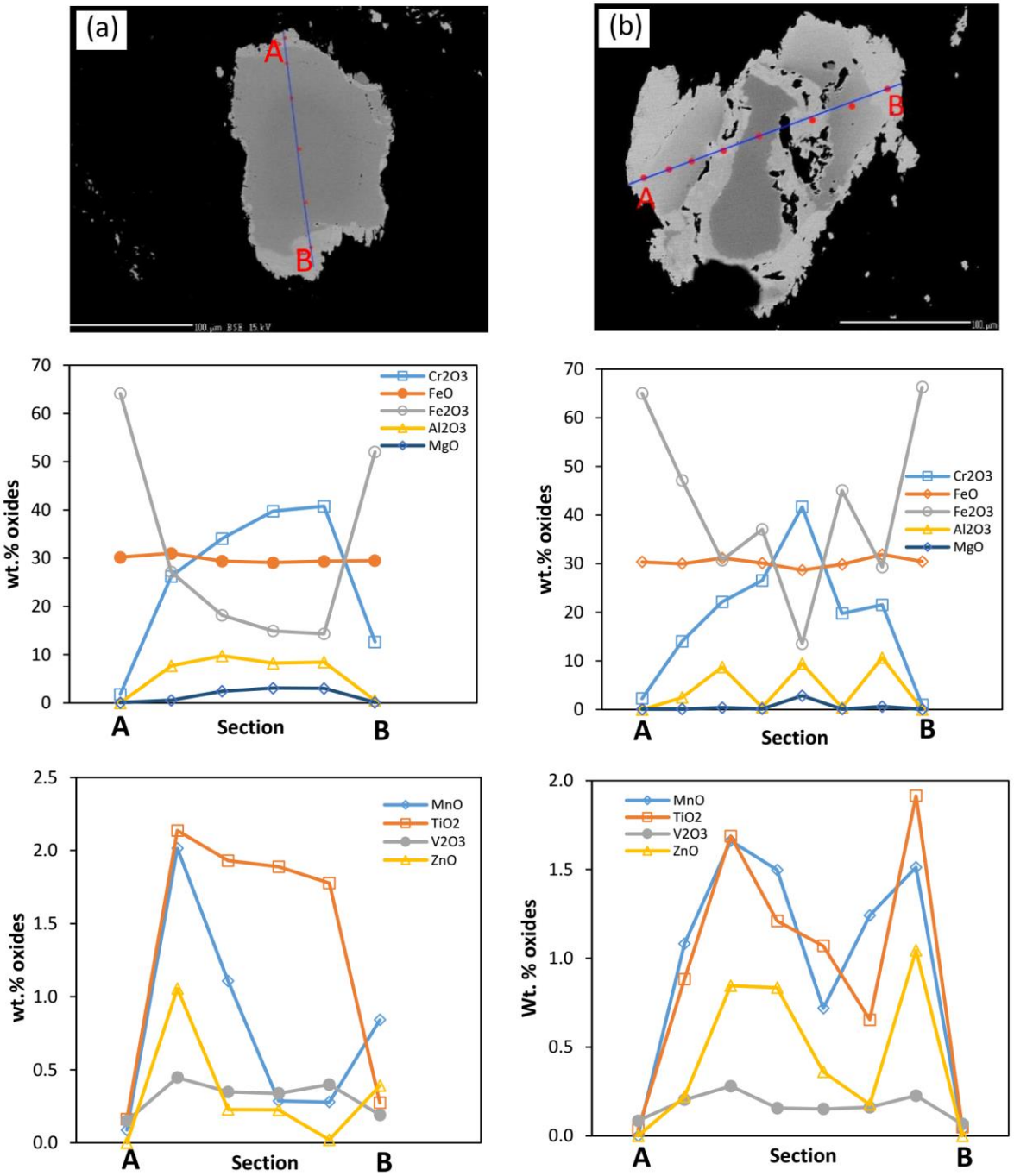


**Fig. 6** Quantitative microprobe profile of major and minor elements across zoned chromite grains. **(a) Type-I:** BSE image of zoned chromite of sample SHB-18-05 showing microprobe traverse A-B; 3 rim present around core; in innermost rim loss of Cr-Al is compensated by enrichment of Fe3+ and loss of Mg by enrichment of Mn; in middle rim loss of Fe3+ is compensated by enrichment of Cr-Al; in the outermost rim we get magnetite. (**b) Type-II:** BSE image of zoned chromite of sample SHB-18-06 showing microprobe transverse A-B; 3 rim present around core; in this case from innermost rim to outermost rim gradual loss of Cr-Al is compensated by enrichment of Fe3+.

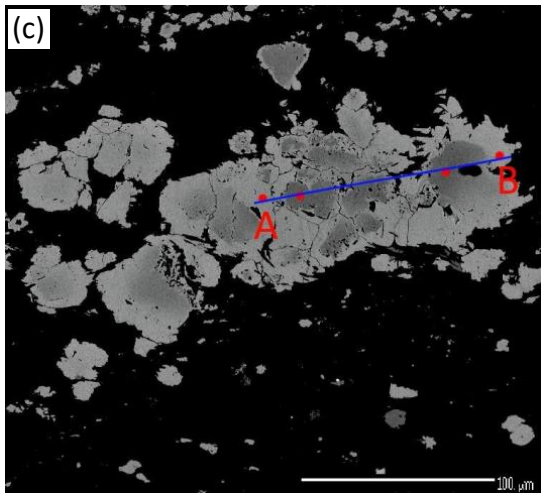


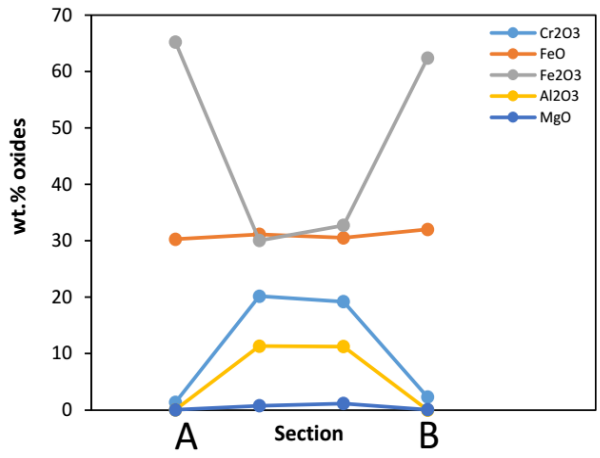


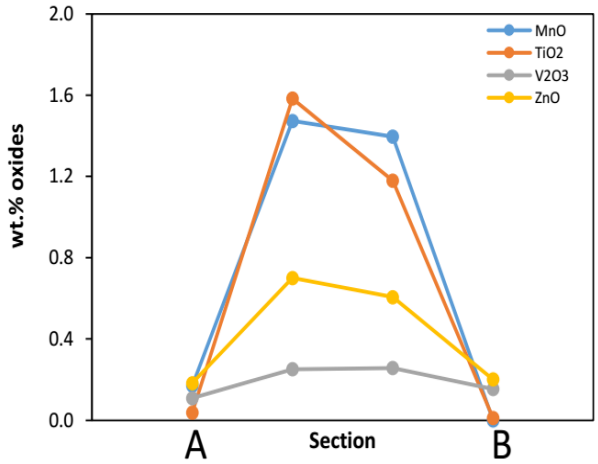


**Fig. 6 (c)** Quantitative microprobe profile of major and minor elements across zoned chromite grains for type-III chromite.

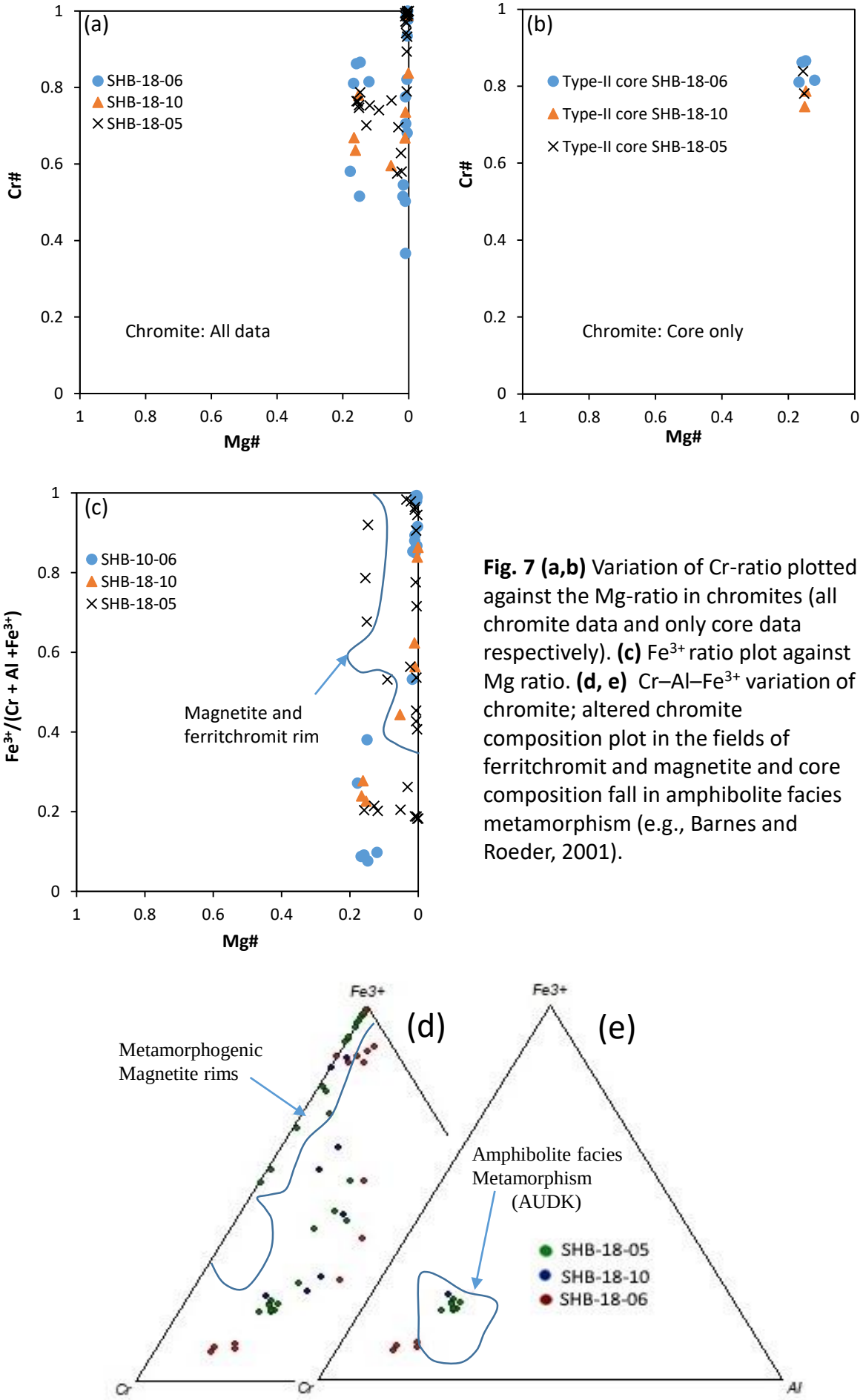


**Fig. 7 (a,b)** Variation of Cr-ratio plotted against the Mg-ratio in chromites (all chromite data and only core data respectively). **(c)** $Fe^{3+}$ ratio plot against Mg ratio. **(d, e)** Cr–Al–$Fe^{3+}$ variation of chromite; altered chromite composition plot in the fields of ferritchromit and magnetite and core composition fall in amphibolite facies metamorphism (e.g., Barnes and Roeder, 2001).

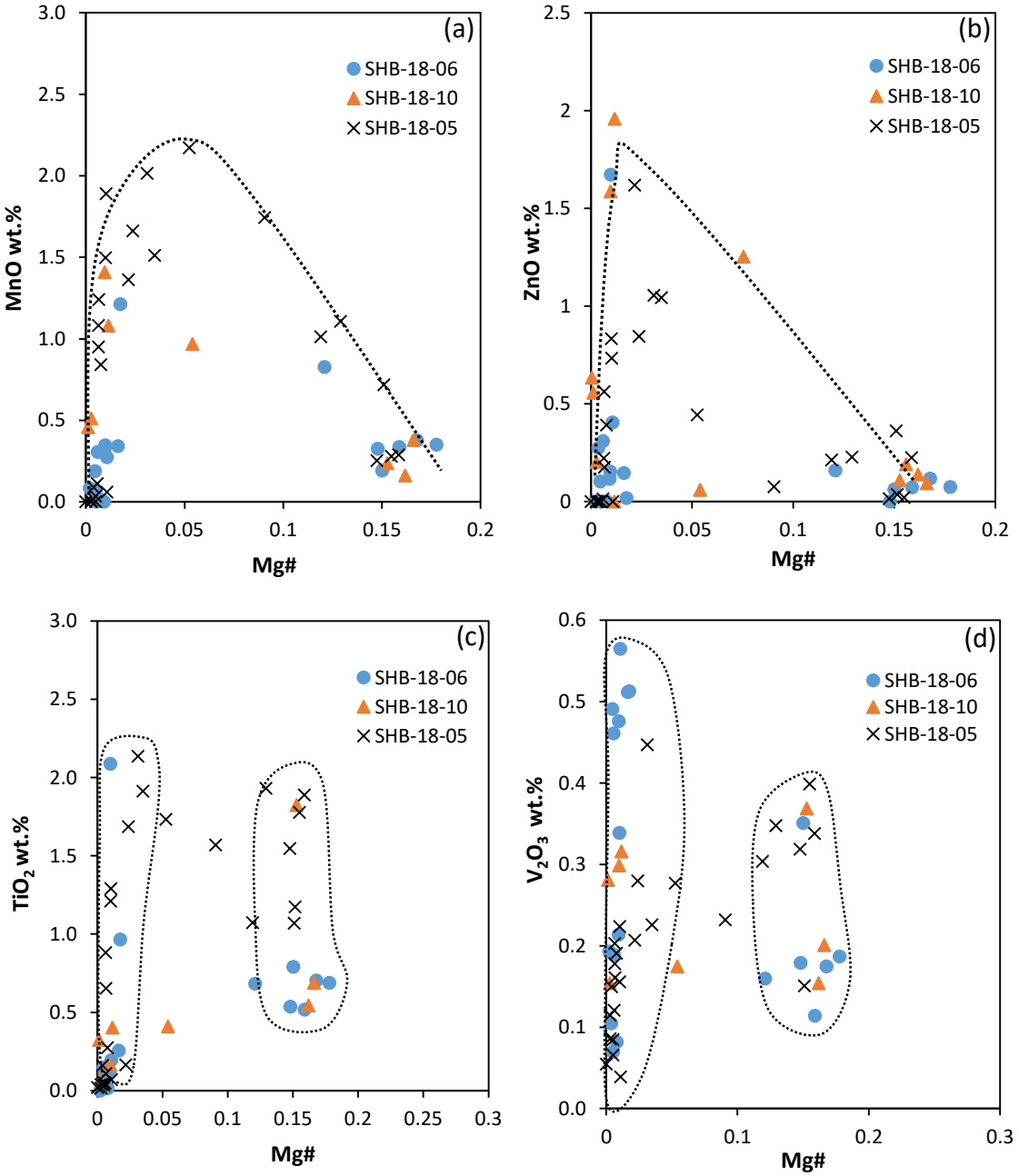


**Fig. 8 (a, b, c, d)** MnO, ZnO, $TiO_2$, $V_2O_3$ oxides wt.% plotted against Mg# respectively.

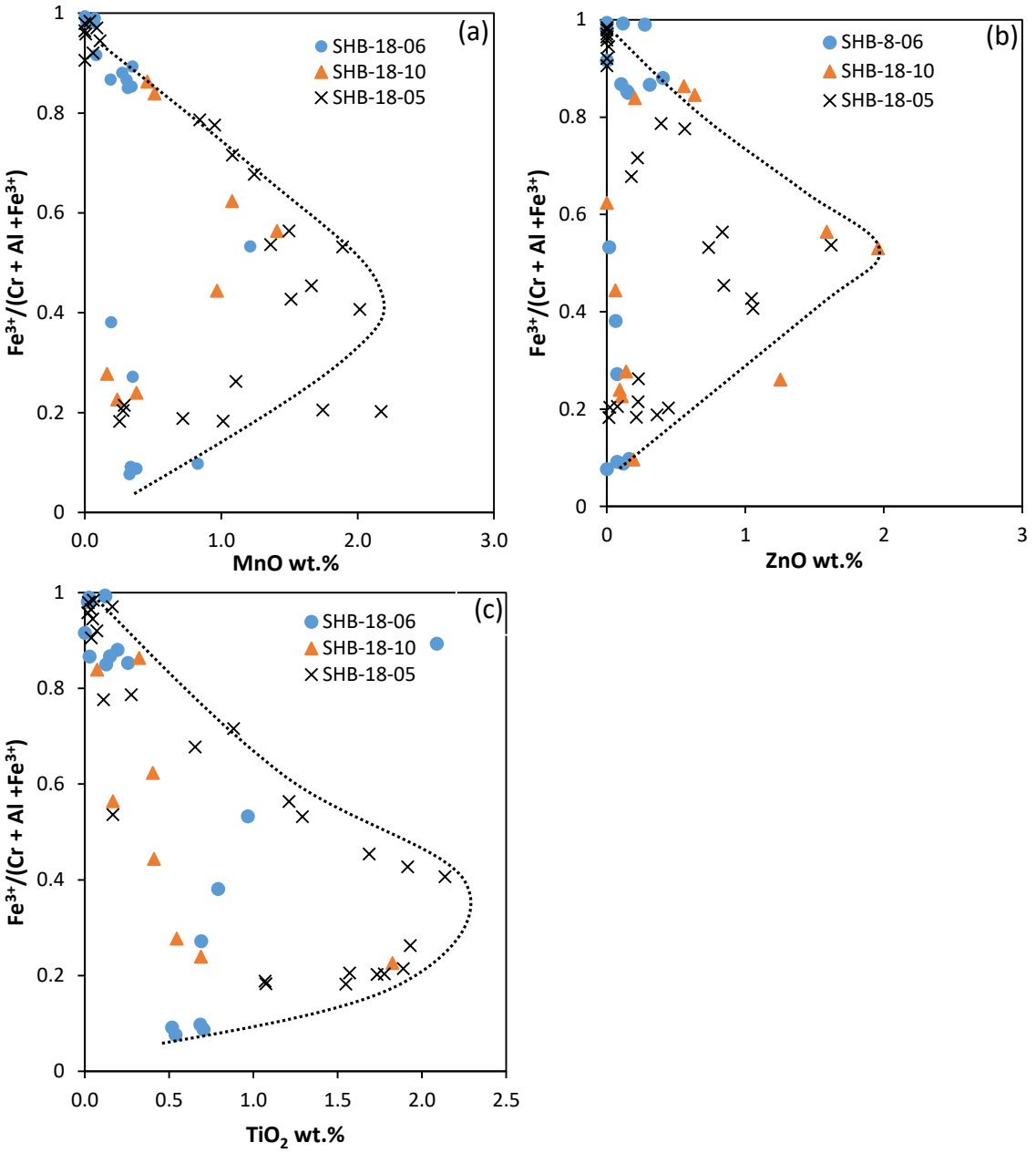


**Fig. 9 (a, b, c)** MnO, ZnO, $TiO_2$ oxides plot against $Fe^{3+}$ ratio respectively.

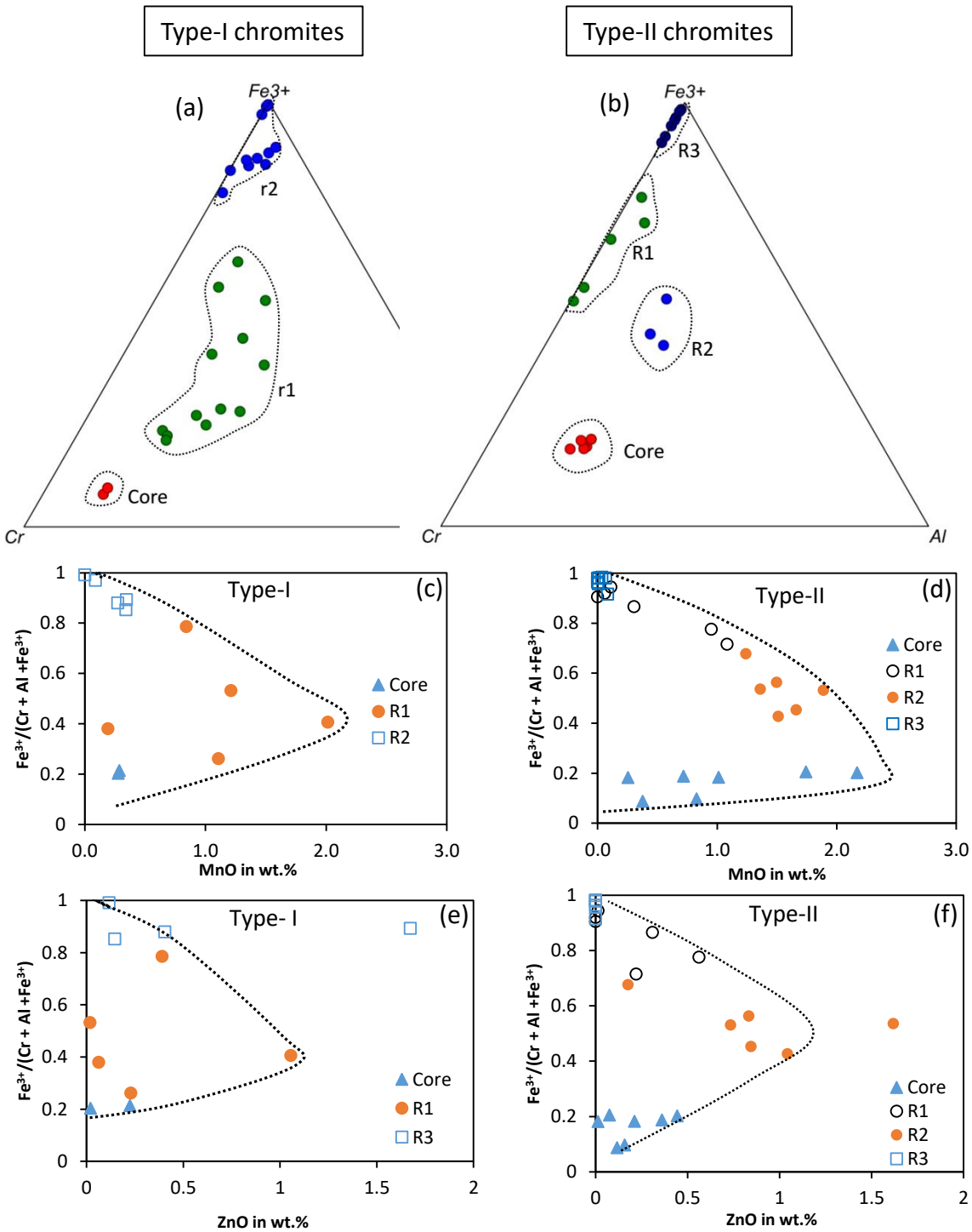


**Fig. 10.** Variation diagrams illustrating chromite composition. **(a, b)** The ternary diagram of Cr-Al-Fe3+ showing composition of accessory chromite in serpentinite (left) Type-I Chromite (red circle= Core, green circle= rim1, blue circle= rim2); (right) Type-II Chromite (red circle= Core, green circle= Rim1, blue circle= Rim2, deep blue circle= Rim3). **(c, d)** Variation of MnO against $Fe^{3+}$ ratio for type-I and type-II chromites. **(e, f)** Variation of ZnO against Mg ratio for type-I and type-II chromites. **(g, h)** Variation of $TiO_2$ against $Fe^{3+}$ ratio for type-I and type-II chromites. **(I, j, k, l, m, n)** Variation of major oxides against Mg# for type-I and type-II chromites.

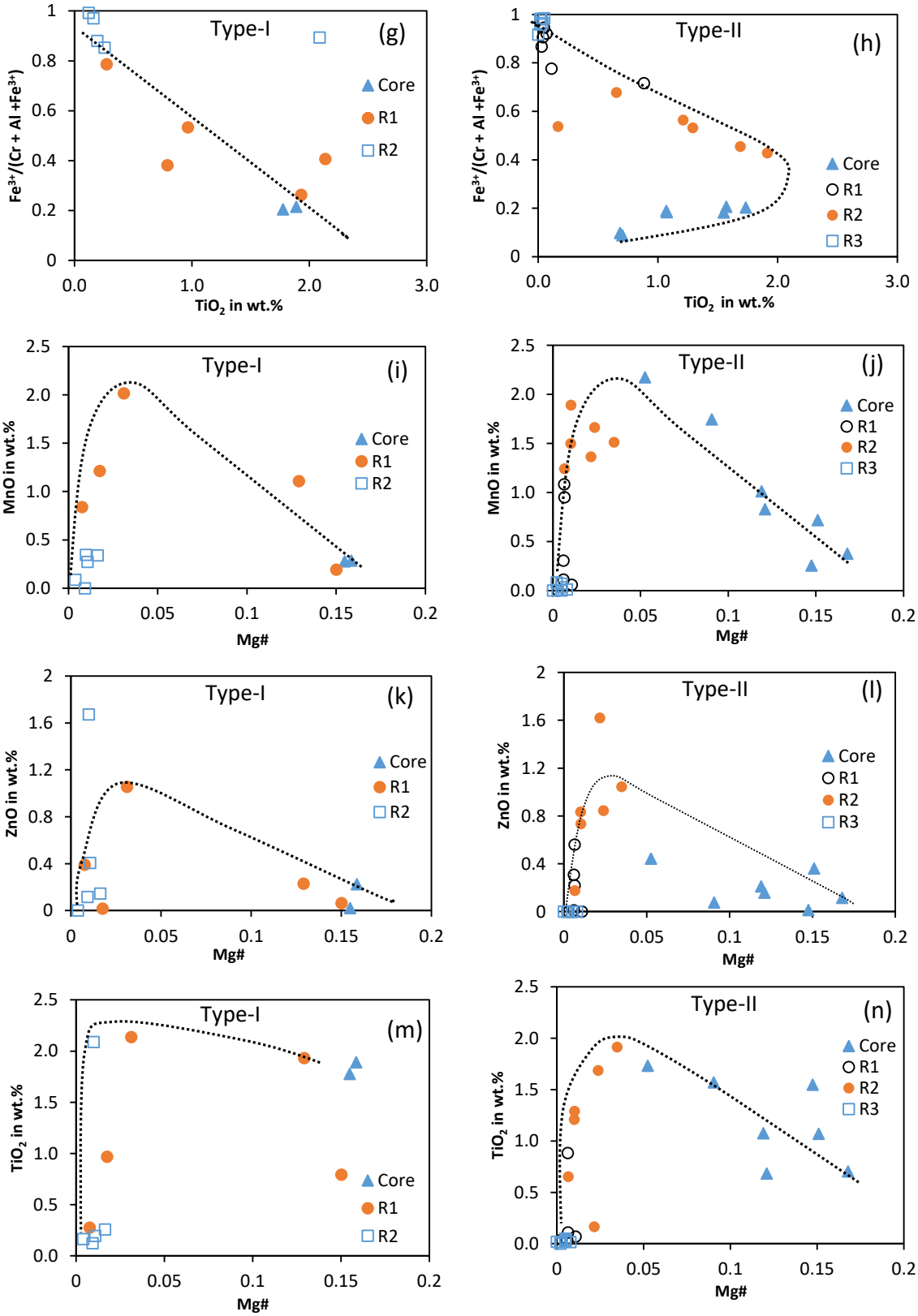


**Fig. 10.** Continued.

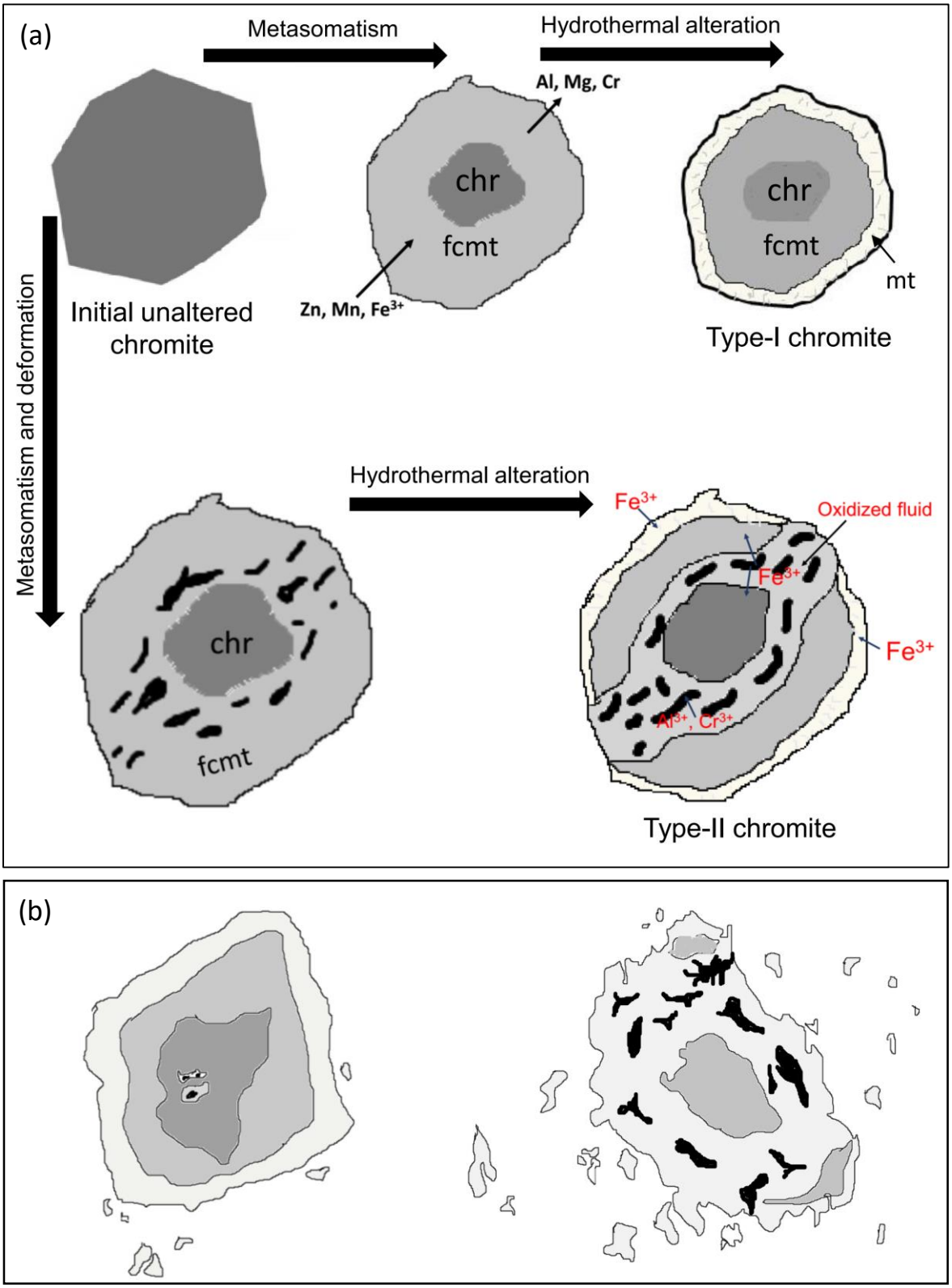


**Fig.11. (a)** Schematic models for formation of type-I and type-II chromites from initial unaltered chromite **(b)** Schematic model for formation of type-IV chromites by fragmentation of type-I and type-II chromites.